

XO-5b: A TRANSITING JUPITER-SIZED PLANET WITH A FOUR DAY PERIOD

CHRISTOPHER J. BURKE¹, P. R. MCCULLOUGH¹, JEFF A. VALENTI¹, DOUG LONG¹, CHRISTOPHER M. JOHNS-KRULL²,
P. MACHALEK^{1,3}, KENNETH A. JANES⁴, B. TAYLOR⁴, MICHAEL L. FLEENOR⁵, CINDY N. FOOTE⁶, BRUCE L. GARY⁷,
ENRIQUE GARCÍA-MELENDO⁸, J. GREGORIO⁹, T. VANMUNSTER¹⁰

(Received 2008 May 15)
Submitted to Astrophysical Journal

ABSTRACT

The star XO-5 (GSC 02959-00729, V=12.1, G8V) hosts a Jupiter-sized, $R_p=1.15\pm 0.12 R_J$, transiting extrasolar planet, XO-5b, with an orbital period of 4.187732 ± 0.00002 days. The planet mass ($M_p=1.15\pm 0.08 M_J$) and surface gravity ($g_p=22\pm 5 \text{ m s}^{-2}$) are significantly larger than expected by empirical M_p -P and M_p -P-[Fe/H] relationships. However, the deviation from the M_p -P relationship for XO-5b is not large enough to suggest a distinct type of planet as is suggested for GJ 436b, HAT-P-2b, and XO-3b. By coincidence XO-5 overlies the extreme H I plume that emanates from the interacting galaxy pair NGC 2444/NGC 2445 (Arp 143).

Subject headings: planetary systems – stars: individual (GSC 02959-00729) – galaxies: individual (NGC 2444, NGC 2445)

1. INTRODUCTION

We report the discovery of a Jupiter-sized planet, XO-5b, that transits the G8V, V=12.1, star GSC 02959-00729 (XO-5) with an orbital period, $P\sim 4$ days. XO-5b provides a valuable addition to the empirical population trends amongst transiting extrasolar planets (Torres et al. 2008), especially at $P>4$ day periods where only four other well characterized transiting planets are known (OGLE-TR-111b, HAT-P-1b, HAT-P-2b, & HD 17156b, Pont et al. 2004; Bakos et al. 2007b; Barbieri et al. 2007, respectively). With a sample of the first six known transiting planets, Mazeh et al. (2005) pointed out the possibility of a linearly decreasing trend of planet mass as a function of increasing orbital period. Torres et al. (2008) and Southworth (2008) have recently revisited this and other relationships amongst the now larger sample of transiting planets analyzed in a homogeneous fashion. As shown in Section 4, XO-5b is one of the few planets that is inconsistent with general trends based on the currently known sample of transiting Jupiter-sized planets.

In Section 2 we describe the photometric and spectroscopic observations that we used to discover and characterize the XO-5, XO-5b system. Section 3.1 describes our spectroscopic determination of the atmospheric properties of XO-5, which we combine with theoretical isochrones to constrain the stellar mass and ra-

dius. The mass estimate of XO-5 is employed along with a high precision transit light curve to measure the radius of XO-5b in Section 3.2. Radial velocity measurements determine the mass of XO-5b as outlined in Section 3.3. In Section 3.4, the database of transit light curves enables refining the transit ephemeris for XO-5b. We conclude in Section 4 how the discovery of XO-5b adds to the understanding of the population of transiting Jupiter-sized planets.

2. OBSERVATIONS

2.1. XO Survey Photometry

McCullough et al. (2005) provides details of the XO survey; additional details of the candidate transiting planet selection process can be found in McCullough & Burke (2007). XO-5b is the fifth Hot Jupiter transiting planet announced by the XO survey (McCullough et al. 2006; Burke et al. 2007; Johns-Krull et al. 2008; McCullough et al. 2008), and was identified as a candidate from the $62^\circ \times 7^\circ$ field of view centered on 8^{h} RA. This field was observed at a 10 min cadence with an overall rms noise, $\sigma = 0.011$ mag, for this V=12.1 star during two seasons: Nov. 2003–Mar. 2004 and Nov. 2004–Mar. 2005. XO-5 is well isolated; XO-5 contributes 90% of the flux in the $75''$ radius aperture used for XO photometry.

Figure 1 shows the XO light curve phased to the period with the most significant transit event identified by the Box-fitting Least Squares algorithm (Kovács et al. 2002). In the phased light curve, two full transit events and five partial events contribute to the detection. After subtracting a transit model (determined from the high precision light curve in Figure 3), the average residual RMS during transit nights is $\sigma = 0.008$ mag (30% lower noise than the average for the entire light curve). Adding in quadrature the Signal to Noise Ratio (SNR) for each transit yields an overall detection $\text{SNR}_{\text{Total}} \sim 12$. It is not routine to follow up all candidates with this low of $\text{SNR}_{\text{Total}}$. However, $\text{SNR}_{\text{Total}}$ is only one of several criteria for selecting candidates (McCullough & Burke 2007; Burke et al. 2007). The efficiency of photometric fol-

Electronic address: cjburke@stsci.edu

¹ Space Telescope Science Institute, 3700 San Martin Dr., Baltimore, MD 21218

² Dept. of Physics and Astronomy, Rice University, 6100 Main Street, MS-108, Houston, TX 77005

³ Johns Hopkins University, Dept. of Physics and Astronomy, Baltimore, MD 21218

⁴ Boston University, Astronomy Dept., 725 Commonwealth Ave., Boston, MA 02215

⁵ Volunteer Observatory, Knoxville, TN

⁶ Vermillion Cliffs Observatory, Kanab, UT

⁷ Hereford Arizona Observatory, Hereford, AZ

⁸ Esteve Duran Observatory Foundation, Montseny 46, 08553 Seva, Spain

⁹ Atalaia, Portugal

¹⁰ CBA Belgium Observatory, Landen, Belgium

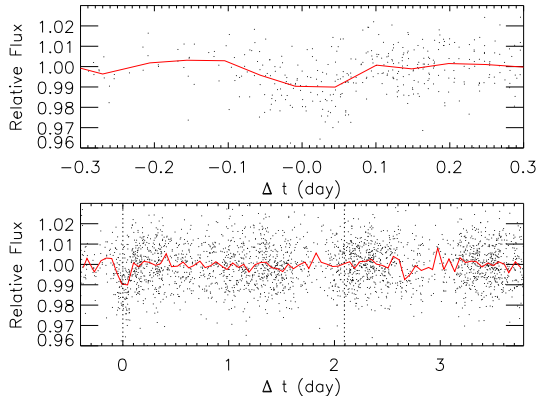


FIG. 1.— Discovery phased light curve from the XO Project data. (Top) The phased light curve around the transit event. (Bottom) The phased light curve over the full orbital period. The individual measurements (*points*) are shown binned (*solid line*) to reduce noise. The transit occurs at $\Delta t = 0.0$ day and any secondary eclipse for a circular orbit would occur at $\Delta t = 2.1$ day (*dotted line*). No secondary eclipse is evident above the noise.

lowup provided by the XO Extended Team is an additional resource of the XO project to aid in following up these lower $\text{SNR}_{\text{Total}}$ candidates.

2.2. XO Extended Team and Follow Up Photometry

The Extended Team (E.T.) provides photometric follow up of XO candidates. The E.T. (M. F., C. F., E. G-M., J. G., F. M., G. M., and T. V.) is a collaboration of professional and amateur astronomers (McCullough et al. 2005, 2006). The E.T. obtains light curves of XO candidates at higher angular resolution and guides the photometric and spectroscopic follow up necessary to classify a candidate as a bona fide planetary companion. Table 1 provides E.T. photometry for XO-5. For the E.T. light curves, the median differential magnitude out of transit provides the flux normalization and the standard deviation out of transit provides the uncertainty in the measurements. Figure 2 shows the E.T. light curves obtained for XO-5b.

On 2008 January 20 we observed a transit event of XO-5b with the 1.8-m Perkins Telescope at Lowell Observatory using the PRISM instrument in imaging mode (Janes et al. 2004). The observations are a continuous series of R-band images covering a $10.8' \times 8.8'$ subarray field of view with 10s exposure time and 30s readout resulting in an overall $t_{\text{cad}} = 40$ s cadence. The detector has $0.36''$ pixels, and the FWHM seeing was $1.8''$. The target was observed over the airmass range, $1.12 \leq X \leq 1.6$, with observations commencing at high airmass. The evening was nonphotometric; several percent transparency variations in raw photometric magnitudes exist around the linear trend with airmass. To remove the transparency variations a differential light curve is calculated employing four other comparable bright stars as comparison. The resulting differential light curve of XO-5 is shown in Figure 3. The out of transit data are limited in duration. Thus, minimizing the scatter during the flat, in-transit portion of the light curve, guided the choice of photometric aperture size and comparison stars. The resulting noise during the in-transit portion is $\sigma_{\text{exp}} = 0.002$ mag for each exposure. This is $\sim 20\%$ higher noise than expected from Poisson, scintillation (Dravins et al. 1997), sky, and read noise. More relevant

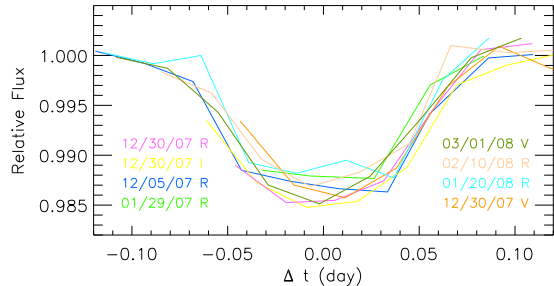


FIG. 2.— Binned light curves from the Extended Team for XO-5. The text in color matches the corresponding light curve and indicates the date and passband of the observations.

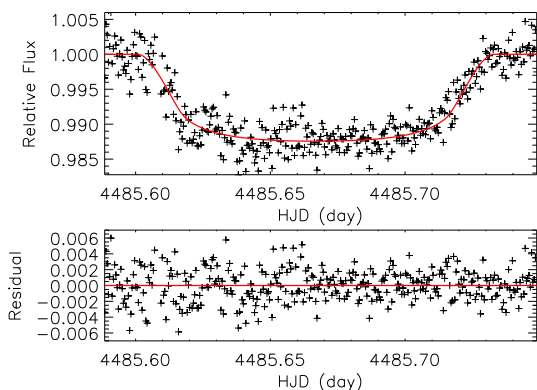


FIG. 3.— Top: Light curve from the 1.8m Perkins Telescope at Lowell Observatory in the R-band (*points*), along with the best-fit transit model in a χ^2 sense during the MCMC analysis (*solid line*). Bottom: Residual of data from the best-fit transit model.

for transit detection and characterization is the photometric noise rate, $\sigma_{\text{pmr}} = \sigma_{\text{exp}} \sqrt{t_{\text{cad}}/60\text{s}} = 0.0016$ mag mn^{-1} , which takes into account the dead time of detector readout. The calibration and photometry was performed in IRAF with a customization in the IRAF phot task to report magnitudes to 10^{-4} precision, rather than the default of 10^{-3} precision.

We obtained photometric B, V, R_C , and I_C magnitudes for XO-5 using a 0.35-m telescope (Table 2). Photometric observations were obtained on three separate nights with 2-6 Landolt star fields (Landolt 1992) interspersed with the XO-5 field in order to define the color and airmass transformation from the instrumental system to the standard system. Each night 20-40 Landolt stars defined the transformation with rms scatter of 0.04, 0.03, 0.02, 0.03 for the *BVRI* passbands, respectively. The resulting standard photometry in Table 2 is the weighted average amongst the three nights. Standard star photometry of XO-5 from *TASS* (Droege et al. 2006) agrees with our photometry. Photometry from *2MASS* (Skrutskie et al. 2006) is also given in Table 2. XO-5 is saturated in *SDSS* (Adelman-McCarthy et al. 2008) images and too faint for the *TYCHO-2* (Høg et al. 2000) database.

2.3. Arp 143 - Potential Archival Measurements

By coincidence, XO-5 lies near the line of sight to the interacting galaxy pair NGC 2444/5 cataloged as Arp 143 in the 'Material Emanating from E Galaxies' group

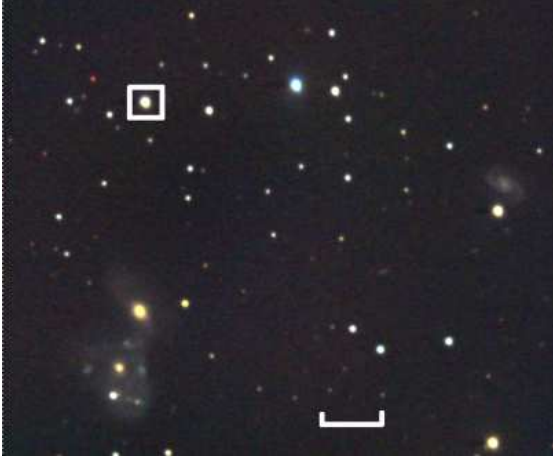


FIG. 4.— False color image for finding XO-5. The box encloses XO-5, and the scale bar indicates 1 arcmin. The finder is ~ 9 arcmin per side, and North is up and East is toward the left. The interacting galaxy pair Arp 143 is visible in the lower left.

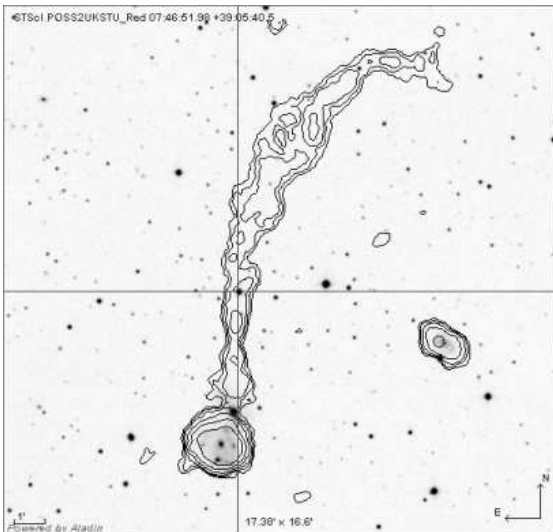


FIG. 5.— Digital Sky Survey image (Red band) of XO-5 (arrow) showing the coincidental H I plume (contour) that emanates from the interacting galaxies Arp 143. The H I emission contours are VLA observations from Appleton et al. (1987).

(Arp 1966). Figure 4 shows a false-color finder chart for XO-5 enclosed by the box along with the Im peculiar galaxy NGC 2445 (patchy blue galaxy) and smoother S0 peculiar galaxy NGC 2444 three arcmin South of XO-5. The VLA has detected one of the largest known (14.5' in extent) H I plumes, which emanates from Arp 143 that directly coincides with XO-5 as shown in Figure 5 (Appleton et al. 1987; Higdon et al. 1997; Hibbard et al. 2001). With a velocity shift of 4000 km s^{-1} , it is improbable that the H I emission from Arp 143 can be attributed to XO-5. Archival observations of Arp 143 may provide long term photometric monitoring or serendipitous transit data for XO-5, possibly constraining ephemeris variability.

2.4. Spectroscopy

After confirmation of the XO transit light curve from E.T. observations (see §2.2), we initiated queue schedule observations of XO-5 with the High-Resolution Spectrograph (HRS), a fiber fed cross-dispersed echelle spec-

trograph (Tull 1998), on the 11-m Hobby-Eberly Telescope (HET) located at McDonald Observatory in order to measure the mass of the planet. HRS observations with an iodine gas cell to yield precise radial velocities commenced on 2007 December 7. Table 3 provides dates of the HRS observations along with the resulting radial velocities. The instrument setup provides $R=63,000$ resolution and covered the wavelength range $4000 < \lambda < 7800 \text{ \AA}$, centered at $\lambda = 5900 \text{ \AA}$. The two-dimensional echelle spectra are extracted using procedures described in Hinkle et al. (2000). Radial velocities for XO-5 are determined in § 3.3.

To measure the stellar parameters of XO-5, we also obtained HRS HET spectra without the iodine absorption cell, using the 5936 \AA and 6948 \AA settings of the cross-disperser to cover the wavelength intervals $5150 < \lambda < 5200 \text{ \AA}$ and $6000 < \lambda < 6200 \text{ \AA}$ at $R=63,000$. Three spectra at each configuration were co-added for analysis. The SNR is 35 and 50 for the co-added spectrum in the blue and red configurations, respectively. The XO-5 stellar parameters are determined in § 3.1.

3. ANALYSIS

3.1. Stellar Properties

A transit light curve and radial velocity measurements do not completely solve the system of stellar and planet properties; these measurements determine the stellar density (Seager & Mallén-Ornelas 2003). Solving for the stellar and planet properties independently requires an additional constraint. Following the procedure of (Burke et al. 2007) in analyzing the transiting planet XO-2b, spectroscopic analysis combined with stellar isochrones provides an estimate of the stellar mass, M_* , and its uncertainty. This prior constraint on M_* enables solving the system completely. We used the Spectroscopy Made Easy (SME) analysis package (Valenti & Piskunov 1996) with refinements from Valenti & Fischer (2005) to determine the spectroscopic properties of XO-5.

Table 2 lists XO-5 stellar parameters from the SME analysis of a single coadded spectrum. The $1\text{-}\sigma$ uncertainties in the stellar parameters given in Table 2 are based on the typical rms scatter in parameters measured in independent, multiple spectra for stars in the SPOCS catalog. XO-5 has an enhanced metal abundance, $[\text{Fe}/\text{H}]=0.25\pm 0.03$, and the effective temperature, T_{eff} and surface gravity, $\log g$ are consistent with a G8V spectral type according to Appendix B of Gray (1992). The empirical T_{eff} , intrinsic color calibrations of Worthey & Lee (2006) predict a color excess, $E(B-V) = 0.03 \pm 0.04$ and $E(V-K) = 0.03 \pm 0.03$ for XO-5. This difference is negligible within the uncertainties, and a typical reddening law predicts $E(V-K)_{pred} = 2.74 \times E(B-V) = 0.08$, lower than the measured excess $E(V-K)$. The extinction map of Schlegel et al. (1998) also measures a modest $E(B-V) = 0.05$ toward XO-5. During the analysis we assume that the standard photometry is free of reddening.

Using the primary observables from the SME analysis (T_{eff} , abundances, and $\log g$) and the apparent V-band magnitude (§ 2.2), we determined M_* and R_* from Y^2 isochrones (Yi et al. 2001), using the procedure of Valenti & Fischer (2005). M_* and R_* depend on the unknown distance to XO-5, thus the probability density function for M_* , R_* , and age are calculated for a se-

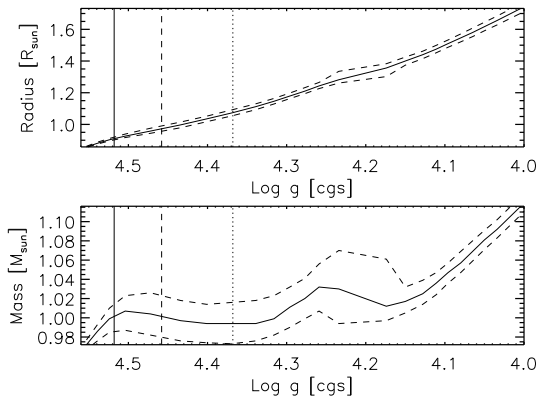


FIG. 6.— Parametric curves for the Radius (*Top*) and Mass (*Bottom*) of XO-5 as a function of the surface gravity from the SME isochrone analysis, respectively (see § 3.1). The SME spectroscopic determination of surface gravity for XO-5 (*solid*), the $1\text{-}\sigma$ internal uncertainty (*dashed*), and the $1\text{-}\sigma$ systematic uncertainty (*dotted*) are shown with vertical lines.

quence of trial distances in steps of 10 pc. Estimates of M_* and R_* from this isochrone analysis provide an additional estimate of $\log g_{iso}$ as a function of distance to XO-5. Figure 6 shows R_* and M_* as a function of $\log g_{iso}$. A lower mass, lower luminosity, younger age, and smaller distance star for XO-5 corresponds to higher surface gravity (left side of Figure 6); whereas, a higher mass, higher luminosity, older age, and larger distance for XO-5 corresponds to lower surface gravity (right side of Figure 6).

A primary goal of the SME analysis is to provide an estimate of M_* and its uncertainty in order to provide a unique solution when fitting the light curve and radial velocity data. The spectrum alone yields an estimate of the stellar gravity, $\log g_{sme}$ that is independent of $\log g_{iso}$. The condition $\log g_{sme} = \log g_{iso}$ and the uncertainty in $\log g_{sme}$ directly yields M_* from the data shown in Figure 6. The solid vertical line in Figure 6 shows $\log g_{sme}$ which corresponds to $M_* = 1.0M_\odot$. The long dashed vertical line in Figure 6 represents the uncertainty of $\log g_{sme}$, $\sigma_{lgg} = 0.06$ dex. This uncertainty is an internal precision of objects in the SPOCS catalog analyzed in a uniform manner. For the purpose of estimating M_* , a more appropriate uncertainty in $\log g$ is determined through comparison of $\log g_{sme}$ from the SPOCS catalog to independent $\log g$ measurements from the literature. Valenti & Fischer (2005) find rms scatter $\sigma_{lgg} = 0.15$ dex by comparing the SPOCS catalog to external catalogs. The dotted vertical line in Figure 6 shows this larger uncertainty in $\log g$. M_* varies weakly with $\log g$, and we adopt an uncertainty of, $\sigma_M = 0.03M_\odot$ for M_* , but also explore the impact a larger, $\sigma_M = 0.07M_\odot$, has on the system parameters.

3.2. Markov Chain Monte Carlo Light Curve Analysis

Ford (2005), Gregory (2005), and references therein provide a thorough discussion of the theory behind Markov Chain Monte Carlo (MCMC) Bayesian analysis along with a practical MCMC implementation for radial velocity planet detection, and Holman et al. (2006) introduced MCMC techniques to the analysis of a transiting planet light curve. To analyze the XO-5b light curve, we follow the MCMC implementation of Burke et al. (2007) where they analyzed the light curve of the transiting

planet XO-2b.

To calculate the Bayesian posterior probability for the system parameters, the likelihood function is given by $e^{-0.5\chi^2}$, where we have assumed the errors are normally distributed, and the data have uniform weights. χ^2 is the squared difference between observations and the analytic transit model of Mandel & Agol (2002). The model assumes negligible eccentricity. The observations are the R-band data from the 1.8m Perkins Telescope shown in Figure 3. To provide the additional constraint necessary to uniquely determine the planet properties, we adopt an informative prior on M_* that is a Gaussian with center $M_* = 1.0M_\odot$ and standard deviation $\sigma = 0.03M_\odot$ (see § 3.1). We adopt uninformative priors for R_* , R_p , and i that are uniform. To improve the efficiency of the MCMC calculation, the computation is done using the set of parameters R_* , $\rho = R_p/R_*$, and the total transit duration from 1st to 4th contact, τ instead of R_* , R_p , and i (Burke et al. 2007). Appendix A of Burke et al. (2007) provides the form of the priors necessary to maintain the uniform priors in R_* , R_p , and i when the calculation is done using R_* , ρ , and τ . The limb darkening coefficients, u_1 and u_2 , of the transit model are allowed to vary. Limb darkening is described by a quadratic law, $I = 1 - u_1(1 - \mu) - u_2(1 - \mu)^2$, where I is the specific intensity normalized to unity at the center of the stellar disk and μ is the cosine of the angle between the line of sight and the surface normal. In practice, we follow Holman et al. (2006) by adopting $a_1 = u_1 + 2u_2$ and $a_2 = 2u_1 - u_2$ as the parameters used in the calculation. The limb darkening coefficients are constrained by requiring the highest surface brightness to be located at the disk center ($u_1 \geq 0.0$), by requiring the specific intensity to remain above zero ($u_1 + u_2 \leq 1.0$), and by not allowing limb-brightened profiles ($u_1 + 2u_2 \geq 0.0$). The final free parameter is the mid-transit time offset, t_o , from the initial ephemeris with a period obtained from analyzing the XO observations and E.T. observations (see § 3.4).

The Markov Chain analysis employs the Metropolis-Hastings algorithm with a normal proposal distribution and a multiple block sampling technique where each step in the chain consists of a number of intra steps updating each individual parameter in turn. Several short, trial chains iteratively yield scale factors of the normal proposal distribution for each parameter with a 25% to 40% acceptance rate for the trial samples. In addition to the choice of R_* , ρ , and τ as the variables for the calculation, a linear transformation between parameters yields an eigenbasis set of parameters with a multi-normal non-covariant relationship that further reduces the mutual degeneracy amongst the parameters (Burke et al. 2007). These transformations yield an efficient MCMC calculation with an autocorrelation length $N_{cor} = 5$ for the chain. The estimate of the posterior probability comes from 7 independent chains of length $N_{chn} = 70000$ with varying initial conditions. This results in an effective length $N_{eff} = N_{chn}/N_{cor} = 14000$.

Figure 7 shows the resulting posterior probability distribution for select system parameters after marginalization over the other parameters. The posterior probability is simply a normalized histogram of the MCMC sample values. We adopt the median as the best sin-

gle point estimate of the posterior probability. The $1\text{-}\sigma$ credible interval for a parameter is given by the symmetrical interval around the median that contains 68% of the samples. Figure 8 shows the joint posterior probability for the stellar limb darkening coefficients, u_1 and u_2 . The constraints on the limb darkening coefficients are not very constraining. Figure 8 shows theoretically calculated limb darkening coefficients in various photometric passbands from Claret (2000) for a star with the physical properties of XO-5. The best estimates for limb darkening coefficients (diamond symbol) from the R-band transit light curve is consistent with the theoretical R-band coefficient (triangle symbol).

Using the SME isochrone analysis, the MCMC samples for R_* translate into distance to and age estimates of XO-5. Similar to the procedure that defines the prior on M_* , The SME isochrone analysis provides a parametric relationship between R_* versus trial distance and age (i.e., for a given stellar radius estimate, the SME isochrone analysis has a best distance and age estimate for the system).

The theoretical planet models of Fortney et al. (2007) characterize the amount of heavy elements (elements heavier than H & He) for a given orbital semi-major axis, R_p , and M_p . The best estimate of R_p for XO-5b is consistent with zero heavy element content, and the $1\text{-}\sigma$ upper limit is $5 M_\oplus$ of heavy elements. Table 5 summarizes the properties of XO-5b.

The uncertainties given in Table 5 for XO-5b and Table 2 for XO-5 represent the internal precision of the experiment. These uncertainties represent the expected scatter of values obtained if the experiment was repeated with similar quality data and identical procedures. Other systematic sources of error are most likely comparable or larger than the internal precision. The sources of systematic error only enter into the prior for M_* . In light of these potential sources of systematic uncertainty, the analysis is repeated with an increased standard deviation of the Gaussian prior on M_* to $\sigma = 0.07 M_\odot$. This larger uncertainty on M_* did not increase the uncertainties in the other parameters beyond the most significant digit as given in Table 2 and Table 5. This indicates the photometric noise rather than uncertainty in M_* dominates the uncertainty in the system parameters.

After fixing the prior on M_* , the light curve analysis yields an additional estimate of $\log g_{mcmc}$ as given in Table 2. $\log g_{mcmc}$ does not differ significantly from the SME based $\log g_{sme}$. We redetermined the stellar properties by fixing $\log g_{sme} = \log g_{mcmc}$ when analyzing the spectra. This reduced $M_* = 0.02 M_\odot$. This variation is within our original uncertainty of M_* . Thus, we did not iterate the MCMC analysis with the SME analysis (Sozzetti et al. 2007).

3.3. Radial Velocity Measurements

We determined the mass of XO-5b using the radial velocity techniques described by McCullough et al. (2006), Burke et al. (2007), and Johns-Krull et al. (2008). We summarize the procedure here, where we derive radial velocity information from the HET spectra (see § 2.4). An iodine gas cell imprints iodine absorption lines on the spectrum of XO-5 and this is compared to a model spectrum to obtain radial velocity shifts with respect to the topocentric frame. We construct model spectra by

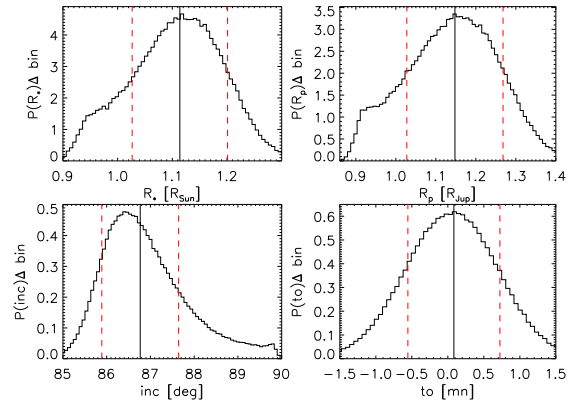


FIG. 7.— Marginalized posterior probability for the XO-5 and XO-5b parameters from MCMC samples. We adopt the median of the posterior probability (solid) vertical line as the point estimate of the parameter. The dashed lines indicate the 68% credible interval.

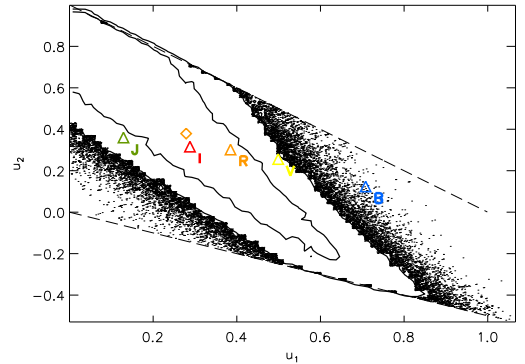


FIG. 8.— Joint posterior probability for the stellar limb darkening coefficients, u_1 and u_2 . The solid contours are isoprobability contours containing 68% and 90% of the MCMC samples. The remaining 10% of the samples lying outside the region of highest probability are also shown (points). The theoretically calculated limb darkening coefficients are shown for various passbands (triangle) along with the best estimate limb darkening coefficients from the MCMC analysis of the R-band transit light curve (diamond). The R-band light curve coefficients are consistent with the theoretically calculated R-band coefficients. The prior limits for the limb darkening coefficients are indicated with dashed lines.

multiplying a very high-resolution FTS spectrum of the Sun (scaled to better match the observed line depths of XO-5) times a very high-resolution FTS spectrum of an iodine gas cell (Cochran 2000) and then convolving the result with a Voigt profile to approximate the line-spread function of the instrument. A radial velocity shift is determined independently for each $\sim 15 \text{ \AA}$ row of the 2-D echelle spectrum of XO-5 over the wavelength range with strong iodine absorption, $5210 < \lambda < 5700 \text{ \AA}$. The individual stellar radial velocity estimates from each of the 15 \AA sections (after transformation to the barycentric frame) determines the stellar radial velocity measurement at each epoch and its associated $1\text{-}\sigma$ uncertainty (see Table 3).

Figure 9 shows the resulting radial velocity curve phased with the XO-5b ephemeris determined from the transits and assuming zero eccentricity. The typical uncertainty per epoch is $\sigma_{RV} = 20 - 40 \text{ m s}^{-1}$, limited mainly by Poisson noise in the spectrum. The radial velocity semi-amplitude, $K = 145 \pm 10 \text{ m s}^{-1}$. This amplitude results in $M_p = 1.15 \pm 0.08 M_J$ for XO-5b, assuming

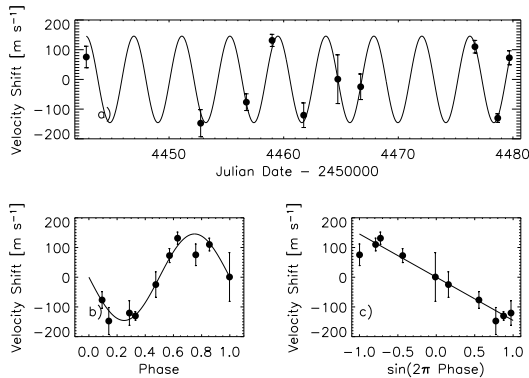


FIG. 9.— a) The radial velocity of XO-5 oscillates sinusoidally with a semi-amplitude $K = 145 \pm 10 \text{ m s}^{-1}$, implying XO-5b’s mass is $1.15 \pm 0.08 M_J$. b) The period and phase of the radial velocities were fixed at values determined by the transits. The mean stellar radial velocity with respect to the solar system’s barycenter has been subtracted. In order to determine K , we used the HET spectra calibrated with an iodine absorption cell (filled circles). c) In this representation of the data, a circular orbit yields a straight line of slope $-K$.

$M_* = 1.0 M_\odot$ for XO-5 and a circular orbit for XO-5b.

3.4. Ephemeris and Transit Timing Variations

The XO, E.T., and Perkins Telescope transit light curves enable refining the ephemeris for XO-5b. The high precision light curve from the Perkins Telescope (see § 2.2), provides the estimate for the mid-transit zero point of the ephemeris as well as the transit model employed to derive mid-transit timing for the other lower precision light curves from the E.T. and XO survey. The MCMC samples from the Perkins Telescope light curve analysis (lower right panel of Figure 7) provide the best estimate and error for the ephemeris zero point, $HJD_o = 2454485.6664 \pm 0.0004$ ($\sigma = 35 \text{ s}$).

To refine the orbital period of XO-5b, the remaining XO and E.T. light curves (E.T. light curves are shown in Figure 2) provide mid-transit timing estimates. The best fitting transit model in a χ^2 sense to the high precision Perkins Telescope light curve (Figure 3) is fit to the other light curves with only mid-transit time and out of transit flux zero point as the only free parameters. The expected variations in the transit model as a function of photometric bandpass is negligible compared to the photometric noise in the E.T. and XO light curves, so the limb darkening coefficients are fixed to the values from analyzing the R-band Perkins light curve. Table 4 provides mid-transit timings along with their uncertainty. The XO observations have 10 min cadence and $\sim 1\%$ photometric noise making transit timing uncertain to 28 min. This uncertainty comes from comparing the a transit model fit a by-eye estimate of the mid-transit timing. Within the uncertainties there is not a significant systematic difference between mid-transit timings estimated by-eye and from the model fit. The much higher quality E.T. light curves have an uncertainty of 4.3 min in mid-transit timing. This uncertainty is estimated from comparing the groups of mid-transit timing observations for the same event but different observers.

With these uncertainties, an ephemeris model with period as the only free parameter results in $\chi^2 = 12.6$ with $\nu = 14$ degrees of freedom indicating the timings are consistent with a fixed period, $P = 4.187732 \pm 0.00002 \text{ day}$.

The ephemeris for XO-5b accumulates a 5 min uncertainty by 2010. Given the large uncertainty in transit mid-point timing from the XO survey data, the period was calculated using E.T. data alone. The earliest, and only, E.T. light curve from the 2006-2007 observing season for XO-5b provides the strongest constraint on the orbital period. The remaining E.T. light curves are from the 2007-2008 observing season for XO-5b. The period derived from E.T. data alone is within $1\text{-}\sigma$ of the determination that includes the XO survey data.

4. DISCUSSION & CONCLUSION

The transit candidate of Mandushev et al. (2005) illustrates the non-negligible potential for triple stars to have transit light curves and radial velocity variations consistent with a planet. However, in the case of XO-5b, attempts to explain the light curve and spectroscopy with a physical stellar triple fail. We employ the Y^2 isochrone appropriate for the the physical properties of XO-5 supplemented with the low-mass stellar isochrone between $0.072 < M_* < 0.5 M_\odot$ from Chabrier et al. (2000), stellar limb darkening coefficients from Claret (2000), the light curve synthesis routine of Wilson (1993), and assume any potential stellar binary has zero orbital eccentricity to model a stellar triple system. The constraints on the transit duration and transit depth from the light curve require $M_* > 0.90 M_\odot$ for the primary of a stellar binary blended with the light of XO-5. The required primary of the stellar binary has $>45\%$ the flux of XO-5 and has a radial velocity semi-amplitude, $K > 18 \text{ km s}^{-1}$. Such a binary would be readily apparent in the spectrum of XO-5 given the narrow spectral features for XO-5, $v \sin i < 3.3 \text{ km s}^{-1}$. We cannot completely rule out the possibility of a line-of-sight faint background binary blended with the light of XO-5 as an explanation for the observations. However, the sinusoidal shape of the radial velocity variations necessitate the line-of-sight binary to have a systemic velocity similar to XO-5 otherwise the radial velocity curve develops asymmetries that are not observed (Torres et al. 2005).

Torres et al. (2008) and Southworth (2008) recently derived transiting planet properties in a uniform fashion in order to further test various trends amongst the transiting planets that have previously been examined with smaller and less homogeneous samples of transiting planets (Mazeh et al. 2005). The larger sample of transiting planets in Torres et al. (2008) still shows a general trend for decreasing M_p with increasing orbital period, but there is significant scatter and some very significant outliers (GJ 436b, HAT-P-2b, and XO-3b). Furthermore, Torres et al. (2008) find a $M_p\text{-P-[Fe/H]}$ relation that reduces the scatter in the $M_p\text{-P}$ relation. At fixed period, the more metal poor stars host higher mass planets. XO-5b has $\Delta M_p = 0.6 \pm 0.08 M_J$ higher mass than then $M_p\text{-P}$ trend defined in Torres et al. (2008). The metallicity correction to the $M_p\text{-P}$ trend found by Torres et al. (2008), $\Delta M_p = -0.14 M_J$ in the case of XO-5b, is opposite sign from what is measured. As commented by Torres et al. (2008), the $M_p\text{-P-[Fe/H]}$ relation does have a scatter larger than observational uncertainties. Thus, additional physical conditions impact the $M_p\text{-P}$ relation, the full variety of Jupiter-class extrasolar planets has not been fully explored, or the trend is more relevant to shorter orbital periods than XO-5b. For in-

stance, Mazeh et al. (2005) propose the M_p -P relation is setup by the thermal evaporation of planets too small to survive the stellar host XUV flux.

Related to M_p , Southworth et al. (2007) and Southworth (2008) show the planet surface gravity, g_p is also correlated with P. The scatter of the g_p -P relation is also larger than the observational uncertainties. XO-5b has a higher g_p than the trend based on previously known extrasolar planets. It is not clear which parameter M_p or g_p is more fundamentally correlated, if at all, with P. Southworth et al. (2007) suggests the g_p -P relation is more fundamental than the M_p -P relation given the direct role g_p has on the evaporation of highly irradiated gas giant planets. Torres et al. (2008) note that the scatter around their g_p -P trend does not correlate with metallicity.

The previously known sample of transiting planets was shown by Hansen & Barman (2007) to separate into two classes by the Safronov number of the planet. The Safronov number, $\theta = 1/2(V_{esc}/V_{orb})^2$, where V_{esc} is the escape velocity from surface of the planet and V_{orb} is the planet orbital velocity, is a measure of the ability of a planet to gravitationally scatter other bodies. Hansen & Barman (2007) and refined by Torres et al. (2008) find transiting planets fall into categories defined as Class I, $\theta \sim 0.07 \pm 0.01$ and Class II, $\theta \sim 0.04 \pm 0.01$. XO-5b, $\theta = 0.1 \pm 0.01$ does not appear to belong to either class, yet it is not as discrepant as the other outlying transiting planets, GJ 436b ($\theta = 0.025$) and HAT-P-2b ($\theta = 0.94$) (Torres et al. 2008). There is some overlap, but the planets with higher metallicity stellar hosts tend to be the Class II objects with lower θ , whereas Class I objects have increasing θ toward lower metallicities. XO-5b does not follow this trend, but has high θ for higher metallicity.

A single object such as XO-5b does not invalidate the trends amongst the Jupiter-class of transiting planets, but illustrates the importance of expanding the number of such objects to fully explore the diversity of this population. Recently, the SuperWASP project announced 10 new transiting planets¹¹. We look forward to the detailed

analysis of these new transiting planets to amplify or diminish the strength of the current trends amongst the close-in transiting planets. The end goal of a large population of transiting planets is to investigate any trends that may directly constrain processes that affect planet formation, migration, and planet survival.

The University of Hawaii staff have made the operation on Maui possible; we thank especially Jake Kamibayashi, Bill Giebank, Les Hieda, Jeff Kuhn, Haosheng Lin, Mike Maberry, Daniel O’Gara, Joey Perreira, Kaila Rhoden, and the director of the IFA, Rolf-Peter Kudritzki. The Hobby-Eberly Telescope (HET) is a joint project of the University of Texas at Austin, the Pennsylvania State University, Stanford University, Ludwig-Maximilians-Universität München, and Georg-August-Universität Göttingen. The HET is named in honor of its principal benefactors, William P. Hobby and Robert E. Eberly. We thank the HET night-time and day-time support staff and the Resident Astronomer telescope operator; we especially thank John Caldwell, Frank Deglman, Heinz Edelmann, Stephen Odewahn, Vicki Riley, Sergey Rostopchin, Matthew Shetrone, and Chevo Terrazas.

We thank Dave Healy, Lisa Prato, and Naved Mahmud for assistance observing; Jim Heasley for assistance on the XO survey; Ron Bissinger, Paul Howell, Franco Mallia, and Gianluca Masi for their contributions in following up XO candidates; and John Hibbard and Phil Appleton for kindly making the H I radio data of Arp 143 available.

This research has made use of the SIMBAD database, operated at CDS, Strasbourg, France; data products from the Two Micron All Sky Survey (2MASS), the Digitized Sky Survey (DSS), and The Amateur Sky Survey (TASS); source code for transit light-curves (Mandel & Agol 2002); and community access to the HET.

XO is funded primarily by NASA Origins grant NNG06GG92G and the Director’s Discretionary Fund of the STScI.

REFERENCES

- Adelman-McCarthy, J. K., et al. 2008, *ApJS*, 175, 297
 Appleton, P. N., Ghigo, F. D., van Gorkom, J. H., Schombert, J. M., & Struck-Marcell, C. 1987, *Nature*, 330, 500
 Arp, H. 1966, *ApJS*, 14, 1
 Bakos, G. Á., et al. 2007, *ApJ*, 656, 552
 Bakos, G. Á., et al. 2007, *ApJ*, 670, 826
 Barbieri, M., et al. 2007, *A&A*, 476, L13
 Burke, C. J., et al. 2007, *ApJ*, 671, 2115
 Chabrier, G., Baraffe, I., Allard, F., & Hauschildt, P. 2000, *ApJ*, 542, 464
 Charbonneau, D., Brown, T. M., Burrows, A., & Laughlin, G. 2007, *Protostars and Planets V*, 701
 Claret, A. 2000, *A&A*, 363, 1081
 Cochran, W. 2000, FTS Spectrum of I2 Cell HRS3 At 69.9 C., ftp://nsokp.nso.edu/FTS_cdrom/FTS50/001023R0.004
 Dravins, D., Lindegren, L., Mezey, E., & Young, A. T. 1997, *PASP*, 109, 173
 Droege, T. F., Richmond, M. W., Sallman, M. P., & Creager, R. P. 2006, *PASP*, 118, 1666
 Ford, E. B. 2005, *AJ*, 129, 1706
 Fortney, J. J., Marley, M. S., & Barnes, J. W. 2007, *ApJ*, 659, 1661
 Gray, D. F. 1992, *The Observation and Analysis of Stellar Photospheres*, by David F. Gray, pp. 470. ISBN 0521408687. Cambridge, UK: Cambridge University Press, June 1992
 Gregory, P. C. 2005, *ApJ*, 631, 1198
 Hansen, B. M. S., & Barman, T. 2007, *ApJ*, 671, 861
 Hibbard, J. E., van Gorkom, J. H., Rupen, M. P., & Schiminovich, D. 2001, *Gas and Galaxy Evolution*, 240, 657
 Higdon, J. L., Rand, R. J., & Lord, S. D. 1997, *ApJ*, 489, L133
 Hinkle, K. H., Joyce, R. R., Sharp, N., & Valenti, J. A. 2000, *Proc. SPIE*, 4008, 720
 Høg, E., et al. 2000, *A&A*, 355, L27
 Holman, M. J., et al. 2006, *ApJ*, 652, 1715
 Kovács, G., Zucker, S., & Mazeh, T. 2002, *A&A*, 391, 369
 Janes, K. A., Clemens, D. P., Hayes-Gehrke, M. N., Eastman, J. D., Sarcia, D. S., & Bosh, A. S. 2004, *Bulletin of the American Astronomical Society*, 36, 672
 Johns-Krull, C. M., et al. 2008, *ApJ*, 677, 657
 Landolt, A. U. 1992, *AJ*, 104, 340
 Mandel, K., & Agol, E. 2002, *ApJ*, 580, L171
 Mandushev, G., et al. 2005, *ApJ*, 621, 1061
 Mazeh, T., Zucker, S., & Pont, F. 2005, *MNRAS*, 356, 955
 McCullough, P. R., Stys, J. E., Valenti, J. A., Fleming, S. W., Janes, K. A., & Heasley, J. N. 2005, *PASP*, 117, 783
 McCullough, P. R., et al. 2006, *ApJ*, 648, 1228
 McCullough, P. R., et al. 2008, *ApJ*, submitted
 McCullough, P. R., & Burke, C. J. 2007, *ASP Conf. Ser.*, *Transiting Extrasolar Planets Workshop*, ed. C. Afonso, D. Wel Drake, & T. Henning (San Francisco:ASP), in press (astro-ph/0703331)

- Pont, F., Bouchy, F., Queloz, D., Santos, N. C., Melo, C., Mayor, M., & Udry, S. 2004, *A&A*, 426, L15
- Schlegel, D. J., Finkbeiner, D. P., & Davis, M. 1998, *ApJ*, 500, 525
- Seager, S., & Mallén-Ornelas, G. 2003, *ApJ*, 585, 1038
- Skrutskie, M. F., et al. 2006, *AJ*, 131, 1163
- Southworth, J., Wheatley, P. J., & Sams, G. 2007, *MNRAS*, 379, L11
- Southworth, J. 2008, *MNRAS*, 386, 1644
- Sozzetti, A., Torres, G., Charbonneau, D., Latham, D. W., Holman, M. J., Winn, J. N., Laird, J. B., & O'Donovan, F. T. 2007, *ApJ*, 664, 1190
- Torres, G., Konacki, M., Sasselov, D. D., & Jha, S. 2005, *ApJ*, 619, 558
- Torres, G., Winn, J. N., & Holman, M. J. 2008, *ApJ*, 677, 1324
- Tull, R. G., MacQueen, P. J., Sneden, C., & Lambert, D. L. 1995, *PASP*, 107, 251
- Tull, R. G. 1998, *Proc. SPIE*, 3355, 387
- Valenti, J. A., & Fischer, D. A. 2005, *ApJS*, 159, 141
- Valenti, J. A., & Piskunov, N. 1996, *A&AS*, 118, 595
- Wilson, R. E. 1993, *New Frontiers in Binary Star Research*, 38, 91
- Worthey, G., & Lee, H. -. 2006, *ArXiv Astrophysics e-prints*, arXiv:astro-ph/0604590
- Yi, S., Demarque, P., Kim, Y.-C., Lee, Y.-W., Ree, C. H., Lejeune, T., & Barnes, S. 2001, *ApJS*, 136, 417
- Zacharias, N., Urban, S. E., Zacharias, M. I., Wycoff, G. L., Hall, D. M., Monet, D. G., & Raftery, T. J. 2004, *AJ*, 127, 3043

TABLE 1
XO, E.T., & Perkins Light Curve Data^a

Heliocentric Julian Date	Light Curve [mag]	Uncertainty (1- σ) [mag]	Filter	N ^b	Observatory
2452961.13135	-0.0033	0.0113	W	1	XO
2452961.13135	-0.0095	0.0113	W	1	XO
2452961.14526	0.0286	0.0113	W	1	XO
2452961.14526	0.0048	0.0113	W	1	XO
2452964.11816	0.0187	0.0100	W	1	XO

^a The complete version of this table is in the electronic edition of this article. The printed edition contains only a sample.

^b Average of N measurements

TABLE 2
Stellar Properties

Parameter	Value of XO-5	Reference
GSC ID	02959-00729	a
RA (J2000.0)	7 ^h 46 ^m 51 ^s .98	a
Dec (J2000.0)	+39° 05' 40".5	a
Galactic Latitude b [deg]	26.94	a
" Longitude l [deg]	180.63	a
V	12.13±0.03	b
(B-V)	0.84±0.05	b
(V-R _c)	0.47±0.05	b
(V-I _c)	0.83±0.05	b
V _{TASS}	12.17±0.06	c
(V-I _c) _{TASS}	0.82±0.08	c
J	10.77±0.02	d
(J-H)	0.33±0.03	d
(H-K)	0.10±0.03	d
Spectral Type	G8V	b
Distance [pc]	270±25	b
μ_α [mas yr ⁻¹]	-32.3±2.7	e
μ_δ [mas yr ⁻¹]	-24.4±5.6	e
Stellar Mass [M_\odot]	1.0±0.03	b,f
Stellar Radius [R_\odot]	1.11±0.09	b
T_{eff} [K]	5510±44	b,f
[Fe/H]	0.25±0.03	b,f
logg [cm s ⁻²]	4.52±0.06	b,f
logg [cm s ⁻²]	4.34±0.07	b,g
$v \sin i$ [km s ⁻¹]	1.8±0.5	b,f
[Na/H]	0.18±0.03	b,f
Stellar ρ [g cm ⁻³]	1.02±0.2	b
Age [Gyr]	8.5±0.8	b

References:

- a) SIMBAD
- b) this work
- c) TASS (Droege et al. 2006)
- d) 2MASS (Skrutskie et al. 2006)
- e) UCAC2 (Zacharias et al. 2004)
- f) SME Spectroscopic Determination (§ 3.1)
- g) Transit Light Curve Determination (§ 3.2)

TABLE 3
XO-5 Radial Velocity Shifts

Julian Date	Radial Velocity Shift [m s ⁻¹]	Uncertainty (1- σ) [m s ⁻¹]
-245000		
4442.7789	75.4	36
4452.7562	-147.4	46
4456.7451	-76.6	28
4458.9892	131.2	20
4461.7447	-120.5	41
4464.7206	0.7	82
4466.7167	-24.8	43
4476.6851	110.0	21
4478.6743	-130.2	14
4479.6874	72.8	24

TABLE 4
Mid-Transit Times

Heliocentric Julian Date -2450000	Uncertainty ($1-\sigma$) [day]	Observatory ID ^b
2999.0114	0.02	XO
3354.9557	0.02	XO
3359.1669	0.02	XO
3375.9428	0.02	XO
3417.8079	0.02	XO
3438.7377	0.02	XO
3442.9195	0.02	XO
4129.7088	0.003	MF
4439.6022	0.003	EGM
4464.7268	0.003	CF
4464.7331	0.003	CF
4485.6730	0.003	CF
4485.6685	0.003	JG
4506.6061	0.003	MF
4527.5427	0.003	JG

^a Observatory ID is author initials, except XO is XO survey data.

TABLE 5
The Planet XO-5b

Parameter	Value
P	4.187732 ± 0.00002 d
t_c	2454485.6664 ± 0.0004 (HJD)
K	145 ± 10 m s ⁻¹
a	0.0508 ± 0.0005 A.U.
i	86.8 ± 0.9 deg
M_p	1.15 ± 0.08 M _J
R_p	1.15 ± 0.12 R _J
g_p	22 ± 5 m s ⁻²
a/R_*	9.81 ± 0.8
R_p/R_*	0.106 ± 0.003
τ	3.13 ± 0.07 hr
Impact parameter, b	0.55 ± 0.09
$\log g_p$	3.35 ± 0.09 cgs
ρ_p	1.02 ± 0.3 g cm ⁻³
$T_{eq} = T_{eff}(R_*/2a)^{1/2}$	1244 ± 48 K
Safronov	0.10 ± 0.01